Fluctuations and anomalous transport (in tokamaks, particularly TEXT)

Plasma Physics and Controlled Fusion, Vol. 30, No. 11, pp. 1479–1491, 1988
Printed in Great Britain.

0741–3335/88 $3.00 + .00
IOP Publishing Ltd. and Pergamon Press plc

FLUCTUATIONS AND ANOMALOUS TRANSPORT (IN TOKAMAKS, PARTICULARLY TEXT)

A. J. Wootton, M. E. Austin[1], R. D. Bengtson, J. A. Boedo, R. V. Bravenec, D. L. Brower[2], J. Y. Chen[3], G. Cima[4], P. H. Diamond[5], R. D. Durst, P. H. Edmonds, S. P. Fan[3], M. S. Foster, J. C. Forster[6], R. Gandy[1], K. W. Gentle, R. L. Hickok[6], Y. X. Hey[3], S. K. Kim[2], Y. J. Kim, H. Lin, N. C. Luhmann[2], S. C. McCool, W. H. Miner, A. Ouroua, D. M. Patterson, W. A. Peebles[2], P. E. Phillips, B. Richards, Ch. P. Ritz, T. L. Rhodes, D. W. Ross, W. L. Rowan, P. M. Schoch[6], D. Sing, E. J. Synakowski, P. W. Terry[7], K. W. Wenzel[8], J. C. Wiley, X. Z. Yang[9], X. H. Yu[9], Z. Zhang[3], S. B. Zheng[9].

Fusion Research Center, University of Texas, Austin, TX 78712.
[1]Auburn University, Auburn, AL 36849.
[2]University of California, Los Angeles, CA 90024.
[3]Institute of Plasma Physics, Hefei, China.
[4]Consiglio Nazionale delle Ricerche, Milano, Italy.
[5]University of California, La Jolla, CA 92093.
[6]Rensselaer Polytechnic Institute, Troy, NY 12181.
[7]Institute for Fusion Studies, University of Texas, Austin, TX 78712.
[8]Massachusetts Institute of Technology, Cambridge, MA 02139.
[9]Institute of Physics, Academy of Science, Beijing, China.

ABSTRACT

Links between turbulent fluctuations and transport processes in tokamaks, particularly in TEXT, are discussed. In the plasma edge probes allow detailed measurements of the quantities required to directly determine the fluctuation driven fluxes. The total flux of particles is well explained by the measured electrostatic fluctuation driven flux. However, a satisfactory model to explain the origin of the fluctuations has not been identified. The processes responsible for determining the edge electron heat flux are less clear. In the confinement region experimental observations are restricted to measurements of density and potential fluctuations and their correlations. Three distinct features have been identified: 1) the ubiquitous broadband turbulence and 2) a quasi-coherent feature, both of which propagate in the electron diamagnetic drift direction, and 3) an ion feature which by definition propagates in the ion drift direction. The characteristics of the measured fluctuations are discussed and compared with the predictions of various models. Comparisons between measured particle, electron heat and ion heat fluxes, and those fluxes predicted to result from the measured fluctuations, are made.

INTRODUCTION

Transport processes in tokamaks are not generally described by the present neoclassical theories, which account for the effects of Coulomb collisions in toroidal geometry. We start by documenting the many disagreements[Hugill, 1983], but note some exceptions where the predictions of neoclassical theory do fit experimental results. It is also well known that real plasmas are rarely quiescent: oscillations arise spontaneously[Liewer, 1985; Robinson, 1986]. In many cases a large number of collective degrees of freedom are excited, defining a state of 'turbulence'. These fluctuations may represent more than harmless oscillations about an equilibrium. We briefly describe how they can affect fluxes of particles and heat, and what measurements are necessary to determine these fluctuation driven fluxes. The main part of the paper then deals with the measurements of the turbulent fluctuation characteristics, the implications for fluctuation driven fluxes, and a comparison between the total and fluctuation driven fluxes. Sections on the plasma edge (defined arbitrarily as r/a > 0.8) and the plasma interior ($r_{q=1} < r < 0.8a$) are included; in each section particle and heat fluxes are considered separately. Here 'a' is the plasma minor radius and $r_{q=1}$ is the radius where the safety factor q=1, taken as the inversion radius of soft X-ray sawteeth[Wesson, 1986]. In some cases the total fluxes are well described by the measured fluctuation driven fluxes, i.e., the turbulent fluctuations can account for transport. The region $r < r_{q=1}$ is mostly avoided because of sparse experimental data and the complicating sawtooth activity.

Starting with the working particle ambipolar flux Γ^i, it is usual and necessary to assume a representation (note superscript i denotes a total, not ion):

$$\Gamma^i = -D^i\nabla n + nv^i \qquad 1)$$

where D^i is the diffusion coefficient, v^i an inward convection velocity and n the density. Γ^i is determined experimentally from spectroscopic measurements of the particle source S (using H_α emission) by invoking continuity:

$$dn/dt = -\nabla\cdot\Gamma^i + S \qquad 2)$$

Behind a limiter, parallel and perpendicular flow[1] can be balanced to derive a diffusion coefficient $D^i \approx 1m^2s^{-1}$. In the plasma interior the coefficients D^i and v^i are separately determined by following the time response of the density profile to a perturbation, e.g., an oscillating gas feed, density sawteeth, or a pellet of solid fuel. The results again show $D^i \approx 1m^2s^{-1}$, while $v^i \approx 10ms^{-1}$; both of these values are larger than the neoclassical values $D^{inc} \approx 1x10^{-3}m^2s^{-1}$ and $v^{inc} \approx 1ms^{-1}$. The experimental values are described as being anomalous (i.e., anomalously large). There are some reported cases, near the plasma axis with low q, where v^{inc} is in agreement with the experimental values[Dnestrovskii, 1984].

Thermal fluxes and diffusivities (χ) are determined from a power balance analysis using the radial profiles of input power, electron temperature T_e, ion temperature T_i, density n, radiation P_{rad}, charge exchange loss P_{cx}, and particle source S. The electron heat flux deduced as a remainder is always anomalously high, being typically 10^3 times the neoclassical prediction. Propagation of locally produced heat pulses gives a value for χ_e a few times that derived from the power balance analysis. Ion thermal fluxes are closer to the neoclassical predictions, but as more detailed information on $T_i(r)$ is becoming available, the ion thermal diffusivity χ_i is found to be up to 10 times χ_i^{nc}.

Neoclassical predictions assume that the density n, electric field E, temperature T, magnetic field b and current density j are stationary. Let the respective fluctuating quantities be represented by $\tilde{n}$, $\tilde{E}$, $\tilde{T}$, $\tilde{b}$ and $\tilde{j}$. Ignoring asymmetries the fluctuation driven radial fluxes (denoted by superscript f) for each species (subscript j) are given by electrostatic (superscript E) and magnetic (superscript b) terms[Ross, 1987]:

Particle flux

$$\Gamma^f_j = \Gamma^{f,E}_j + \Gamma^{f,b}_j \qquad 3)$$

$$\Gamma^{f,E}_j = \frac{\langle\tilde{E}_\theta\tilde{n}_j\rangle}{B_\phi} \qquad 4)$$

$$\Gamma^{f,b}_j = -\frac{\langle\tilde{j}_\parallel\tilde{b}_r\rangle}{(eB_\phi)} = g_1\left(\frac{\tilde{b}_r}{B_\phi}\right) \qquad 5)$$

Energy flux

$$Q^f_j = Q^{f,E}_j + Q^{f,b}_j \qquad 6)$$

$$Q^{f,E}_j = \frac{3}{2}k_b\, n\,\frac{\langle\tilde{E}_\theta\tilde{T}_j\rangle}{B_\phi} + \frac{3}{2}k_b\, T_j\,\frac{\langle\tilde{E}_\theta\tilde{n}_j\rangle}{B_\phi} \qquad 7)$$

$$Q^{f,b}_j = g_2\left(\frac{\tilde{b}_r}{B_\phi}\right) \qquad 8)$$

Here k_b is Boltzmann's constant, subscripts r, θ, ϕ, $\parallel$, $\perp$ refer to radial, poloidal, toroidal, parallel and perpendicular to the magnetic field, and $\langle\ \rangle$ denotes an ensemble average (we have assumed a circular cross sectioned plasma). The exact form for the functions $g_1(\tilde{b}_r/B_\phi)$ and $g_2(\tilde{b}_r/B_o)$ depend on the exact plasma parameters[Liewer, 1985], but typically $g_1(\tilde{b}_r/B_\phi)$ is negligible and

$$g_2(\frac{\tilde{b}_r}{B_\phi}) \approx \pi R\, v_{the} (\frac{\tilde{b}_r}{B_\phi})^2 \quad \text{in a collisionless plasma} \qquad 9)$$

$$g_2(\frac{\tilde{b}_r}{B_\phi}) \approx \chi_{e\|} (\frac{\tilde{b}_r}{B_\phi})^2 \quad \text{in a collisional plasma} \qquad 10)$$

with v_{the} the electron thermal velocity, $\chi_{e\|}$ the classical parallel electron thermal diffusivity, and R the plasma major radius.

It is customary to split the total energy flux Q_j into a conducted heat flux q_j and a convected flux $5/2\, k_b T_j \Gamma_j$:

$$Q_j = q_j + \frac{5}{2} k_b T_j \Gamma_j \qquad 11)$$

so that

$$q_j = \frac{3}{2} k_b\, n \frac{<\tilde{E}_\theta \tilde{T}_j>}{B_\phi} + g(\frac{\tilde{b}_r}{B_\phi}) - k_b T_j \Gamma_j \qquad 12)$$

There is disagreement in the literature as to whether the factor in the electrostatic component of the energy flux (Eq. 7) is 3/2 or 5/2: the difference is related to the contribution made by the turbulence to the energy source $<E_\perp . j_\perp>$[Ross, 1987].

If we could measure $\tilde{n}$, $\tilde{E}$, $\tilde{T}$ and their correlations throughout the plasma volume, we could identically measure the electrostatic components of the various fluctuation driven fluxes. We can do this at the plasma edge using probes. For example the electrostatic particle flux $\Gamma^{f,E}$, and therefore the convected part of the energy flux, is measured as a function of frequency $\omega/2\pi$ in terms of the root mean square (rms) fluctuation levels[Powers, 1974]:

$$\Gamma^{f,E}(\omega,k) = \tilde{n}_{rms}\, \tilde{\phi}_{rms}\, |\gamma_{n\phi}|\, k_\theta(\omega)\, \sin(\alpha_{n\phi}(\omega))/B_\phi \qquad 13)$$

where k_θ is the measured poloidal wave number, $\tilde{\phi}$ is the measured fluctuating plasma potential ($=\tilde{E}_\theta/k_\theta$), $\gamma_{n\phi}$ is the measured coherence between $\tilde{n}$ and $\tilde{\phi}$, and $\alpha_{n\phi}$ the measured phase between $\tilde{n}$ and $\tilde{\phi}$. To determine the electrostatic energy flux $Q^{f,E}$ we need the correlation between $\tilde{E}$ (or $\tilde{\phi}$) and $\tilde{T}$, which is not generally known. However, an upper bound can always be placed by assuming perfect correlation (i.e. $\gamma_{T\phi}=1$, $\sin(\alpha_{T\phi})=1$).

To estimate the magnetic components $\Gamma^{f,b}$ and $Q^{f,b}$ we should measure $\tilde{j}_{\|}$ and $\tilde{q}_{\|}$, but this is not done. Instead $\tilde{b}$ is measured, and then models applied (e.g., Eq. 9 or 10) to derive the fluxes. In the plasma edge we can measure or estimate all the required terms, derive the turbulence driven fluxes, and compare them with the total measured fluxes Γ^i and Q^i to determine if the measured fluctuations play an important role in plasma transport processes.
In the plasma confinement region the diagnostic problem is more difficult, because the high parallel heat flux precludes the use of material probes. Scattering of laser light [e.g., Brower, 1987a] is used to determine the spectral power density distribution function $S(k,\omega)$, where

$$<|\tilde{n}|^2> = (2\pi)^{-4} \int dk^3 d\omega S(k,\omega) \qquad 14)$$

From this measurement we can determine the frequency integrated spectral density function $S(k) \propto \tilde{n}(k)^2$, the wave number integrated spectral density function $S(\omega) \propto \tilde{n}(\omega)^2$, and various spectral averages (e.g. $\bar{v}_{ph} = \Sigma_{\omega,k}(\omega/k)S(k,\omega)/\Sigma_{\omega,k}S(k,\omega)$, $\bar{k} = \Sigma_{\omega,k}kS(k,\omega)/\Sigma_{\omega,k}S(k,\omega)$). Typically $0<k_\perp<1.5mm^{-1}$ (where $\mathbf{k}_\perp = \mathbf{k}_r + \mathbf{k}\theta$). With heterodyne detection, the electron drift direction and ion drift direction spectral density functions (S_e and S_i) can be separated[Brower, 1987b]. Another diagnostic, the heavy ion beam probe (HIBP) [e.g., Hallock, 1987], allows simultaneous measurements of both density and potential fluctuations over a large range of k, $0<k_\perp<5mm^{-1}$, together with $\alpha_{n\phi}$ and $\gamma_{n\phi}$ for $0<k_\perp<0.5mm^{-1}$. While the FIR scattering measures the k spectrum directly, both the HIBP and Langmuir probes utilize a two point correlation technique. Unfortunately no diagnostics yet exist which give information on $\tilde{T}$ in the confinement region, and the only information on $\tilde{b}$ is inferred from runaway electron confinement properties. Thus we are restricted to directly measuring only $\Gamma^{f,E}$.

Information on $\Gamma^{f,b}$, $q^{f,E}$ and $q^{f,b}$ must come from using what we can measure (e.g., $\tilde{n}$ (k,ω) and $\tilde{\phi}$(k,ω)) in various models.

THE PLASMA EDGE

a) Particle fluxes

We start by presenting some properties of the electrostatic fluctuations, which we will show later are largely responsible for particle confinement. Figure 1 [Ritz, 1987a] shows S(k,ω) obtained with a Langmuir probe and FIR scattering at the edge of TEXT. The results demonstrate the broadband nature of the fluctuations ($\Delta\omega/\bar{\omega} \approx \Delta k_\theta/\bar{k}_\theta \approx 1$) with $\bar{k}_\theta \rho_s \approx 0.05$-$0.1$. Here ρ_s is the gyroradius using T_e and the ion mass, and is a characteristic radial scale length. The fluctuations propagate in the electron drift direction, with $\bar{v}_{ph} \approx 3\times10^3 ms^{-1}$. The frequency broadening demonstrates the turbulent nature, and three-wave interactions play an important role in determining the spectral shape[Ritz, 1987b]. For r > a the fluctuations propagate in the ion drift direction, i.e., there is a velocity shear layer at r ≈ a.

We wish to correlate properties of the electrostatic fluctuations with particle confinement. Figure 2 shows the particle confinement time τ_p for 4 different machines; JET[Cordey, 1985], ALCATOR[Marmar, 1978],JT-60[Yamada, 1987] and TEXT[Rowan, 1987]:

$$\tau_p = \frac{\int n dV}{\int \Gamma^i dS_\phi} \qquad 15)$$

where V is the plasma volume and S_ϕ the plasma surface area, and the integrals. The integrals are carried out to r = a. Both τ_p and the line of sight average density $\bar{n}_e$ are normalized to the values where τ_p is maximum. With this normalization the four very different machines demonstrate a similar dependence of τ_p on $\bar{n}_e$, suggesting a common driving mechanism. Additional heating often reduces τ_p, but the combination of separatrix and additional heating can overcome the loss of confinement if certain power threshold conditions are satisfied (the H mode [Wagner, 1986]).

On TEXT a comparison between the total and electrostatic fluctuation driven fluxes has been made[Rowan, 1987]. The scalings and absolute magnitudes of $\Gamma^{f,E}$ (determined using Eq. 13, with data similar to that shown in Fig. 1) and Γ^i at r=a, or equivalently $\tau_p^{f,E}$ and τ_p^i, agree. Figure 3 shows an example of the comparison of the radial dependencies of the fluxes near and behind the limiter. The ordinate ρ is the normalized flux surface radius. A simple model for parallel flow to the limiter[Howe, 1985] has been used to obtain the perpendicular component Γ^i. The approximate agreement demonstrates that the measured turbulent fluxes account for an important part, if not all, of the total particle fluxes in the edge. Some interesting, unresolved problems arise from the shape of the $\Gamma^{f,E}(\rho)$ curve, which apparently violates continuity. Asymmetries influence the results, but do not change the major conclusion.

Experimental results from the ISX-B tokamak[Hallock, 1987] show neutral beam heating (L-mode) reduces τ_p and increases $\Gamma^{f,E}$. Therefore, the degradation in confinement is associated with an increase in $\Gamma^{f,E}$. No results are available with the H-mode, but it seems reasonable to suppose that the improvement in particle confinement is associated with a decrease in $\Gamma^{f,E}$ and mechanisms to explain this should be investigated.

An association between negative radial electric field E_r and improved confinement, and positive E_r and degraded confinement, is suggested with neutral beam injection, radio frequency heating, and biased limiter experiments[Phillips, 1987]. Biased limiter results on TEXT show a correlation between reducing E_r (i.e., more negative than the usual value), decreasing Γ^i, (improving τ_p and impurity confinement), and decreasing $\Gamma^{f,E}$. Again, the correlation between total and electrostatic fluctuation driven flux is identified.

b) Energy fluxes

Figure 4a) shows the radial variations of $\tilde{n}/n$, $\tilde{\phi}/(k_bT_e)$, and $\tilde{b}_r/B_\phi$ for a particular discharge condition in TEXT. Measurements show $\tilde{T}_e/T_e \approx 0.4\ \tilde{n}/n$. Note $\tilde{\phi}/(k_bT_e) \neq \tilde{n}/n$. From these results, and the respective correlations, we can deduce the radial variations of the terms in the energy flux Q_e (Eq. 11). The radial profiles are shown in Figure 4b) and 4c). Also shown are the radial profiles of the total fluxes deduced from the power balance analysis and limiter thermography (the latter confirms the parallel heat flux flowing to the limiter). We find, assuming poloidal and toroidal symmetry, that >50% of Q^{tot}_e is accounted for by electrostatic convection ($5/2\ k_bT_j\Gamma^{f,E}_j$), <20% by electrostatic conduction ($q^{f,E}_e$, Eq. 12), and <0.1% by magnetic conduction (Eq.10). Because of the large uncertainties in the power balance analysis, convection could explain all of Q^{tot}_e. At lower densities[Ritz, 198c] the power balance analysis is more certain, (except for the possibility that non-thermal electrons affect the parallel loss term for r > a) and shows we cannot account for all of Q^{tot}_e by electrostatic fluctuations. In particular $q^{tot}_e > q^{f,E}_e$, as in Figure 4c). Asymmetries do exist and may play an important role in the analysis.

c) Theoretical models

Some of the measured fluctuation characteristics are given in Table 1, together with the predictions of two models. In one model (drift waves[Terry, 1985]) the turbulence is driven by ∇n, and in another (rippling mode[Garcia, 1985]) by $\nabla\eta$, the resistivity gradient. Neither model can reproduce all of the observed characteristics. In particular the ∇n model cannot predict the non-Boltzmann like behavior ($\tilde{\phi}/(k_bT_e) \neq \tilde{n}/n$), the phase angle $\alpha_{n\phi}$, the radial dependence or the scaling of the fluxes. The $\nabla\eta$ model fairs better, failing only in its prediction of the high poloidal mode numbers $\overline{m} \approx 50$ which are measured. Unless $\overline{m} \approx 5$ is used in the $\nabla\eta$ model, the predicted particle fluxes are too small.

THE PLASMA INTERIOR

a) Turbulence characteristics

Less detailed information is available on interior turbulence, although confinement properties are better known. In general the exact parameters required to determine the fluctuation driven fluxes are not available, and we must interpret the limited data using analytic models. The first part of this section summarizes the characteristics of the turbulence. For simplicity of presentation some edge properties determined with FIR scattering are also included here, although they should properly have been considered above. We then discuss particle, electron heat, and finally ion heat, transport.

Figure 5 is a characterization of the results obtained with FIR scattering[Brower, 1987a] in which the density of points is intended to represent the value of $\tilde{n}/n$. Also shown are the scattered power (P_s) frequency spectra for $k_\perp = 1 mm^{-1}$ at various locations. At the plasma periphery the broadband turbulence ($\Delta\omega/\bar{\omega} \geq 1$, $\Delta k/\bar{k}_\theta > 1.5$, both FWHM) is found, with $\bar{k} \propto B_\phi^{0.6}\ I_p^{-0.2}$ and $\bar{k}_\theta\rho_s \approx 0.15$. The amplitude decreases towards the plasma center. Very little, if any, explicit dependence of $\bar{k}$ on ion mass is found, but the mass scaling of Δk and $\tilde{n}$ is being investigated. The fluctuations propagate in the electron diamagnetic drift direction with a typical phase velocity $\bar{v}_{ph} \approx 3x10^3 ms^{-1}$. This is significantly greater than expected for drift waves in a rotating plasma, $v_{ph} = v_{de} + v_\theta + v_\phi\ k_\phi/k_\theta \approx 1x10^3 ms^{-1}$ (v_{de} is the electron diamagnetic drift velocity = $k_bTe/(eB_\phi L_n)$, L_n is the density scale length, v_θ the poloidal rotation velocity taken as the neoclassical value, and the toroidal rotation velocity v_ϕ is ignored). This broadband turbulence is up-down asymmetric at the plasma edge[Brower, 1985a], the asymmetry depending on the direction of the plasma current (the exact scaling of $\tilde{n}/n$ with $\bar{n}_e$ is different at the top and bottom). Such an asymmetry can result from a toroidal asymmetry in the system, e.g., the poloidal ring limiter or the toroidal field ripple. Experiments employing movable limiters show the limiter geometry has an important role in determining the edge density fluctuations, and thus presumably edge transport. This suggests that differences should be expected in edge turbulence and perhaps transport for poloidal ring, toroidal belt and separatrix limited discharges.

In addition to the broadband turbulence a quasi-coherent mode [Brower, 1987a; Brower, 1985b] ($\Delta\omega/\bar{\omega} \approx 0.1$,

$\Delta k/\bar{k}_\theta \approx 0.7$) has been identified at the inner equator, also propagating in the electron diamagnetic drift direction with $\bar{v}_{ph} \approx 1x10^3 ms^{-1}$. This velocity is much closer to the expected value of $\approx 1x10^3 ms^{-1}$, suggesting the measured $\bar{v}_{ph}$ for the broadband feature might be a result of modes propagating in the plasma rest frame with velocity > v_{de}. Scaling studies of this quasi-coherent feature show $\bar{k} \alpha B_\phi^{0.7} I_p^{-0.2}$, $\bar{k}_\theta \rho_s \approx 0.6$. The scaling of $\tilde{n}/n$ (αB_ϕ^{1}) is very different from the broadband feature scaling (where $\tilde{n}/n \alpha B_\phi^{-1}$). Although seen in the interior, this feature may be largest at the inner equator, which is presently inaccessible.

A third feature, broadband and propagating in the ion drift direction, has also been identified[Brower, 1987a; Brower, 1987b]. The spectral power density in the ion feature (S_i) relative to that in the broadband electron drift feature (S_e) increases with increasing $\bar{n}_e$. Ignoring complications which arise in the analysis of S_e and S_i from any plasma mass rotation, S_i/S_e increases from 0.08 to 0.5 as $\bar{n}_e$ is increased from 2 to $8x10^{19} m^{-3}$, with B_ϕ = 2.8T and I_p = 400KA. This is discussed in more detail later (Fig. 11). With the above picture it is clear that spatial asymmetries are important, and it is unlikely that any single model will explain all the details of the interior fluctuations.

Figure 6 shows the spatial dependence of $\tilde{n}/n$ for the broadband feature in TEXT where good spatial resolution is obtained using the HIBP. Also shown are the predictions of 'mixing length' models for drift wave turbulence. These predict $\tilde{n}$ saturates when the convection of perturbed density balances the convection of average density which drives the mode, i.e., when $(\tilde{n}/n) \approx \tilde{\phi}/(k_b T_e) \approx 1/(k_r L_n)$. The depicted ranges correspond to uncertainties in the measured plasma parameters. For slab geometry ($k_r \approx \rho_s^{-1}(L_n/L_s)^{1/2}$) we have $(\tilde{n}/n)^{slab} = \rho_s L_n^{-3/2} L_s^{1/2} \approx 3\rho_s/L_n$ [Perkins], while for toroidal geometry ($k_r \approx k_\theta \hat{s}$) we have $(\tilde{n}/n)^{tor} \approx 1/(k_\theta \hat{s} L_n)$ [Similon, 1984]. In these expressions $L_n = -n(dn/dr)^{-1}$, $L_s = Rq/\hat{s}$, and $\hat{s} = r/q.\partial q/\partial r$. Insufficient information exists at all radii to use measured values of k_θ (which affects $(\tilde{n}/n)^{tor}$), so we have invoked the drift wave scaling $\bar{k}_\theta \rho_s \approx c$, with c an experimentally determined constant. Both at $\rho \approx 1$ (Langmuir probes, HIBP, FIR) and at $\rho \approx 0.6$ (HIBP) we measure $c \approx 0.1$. The better representation is then given by $(\tilde{n}/n)^{slab}$. However, if $c \approx 0.4$, a value found in some other tokamaks([Liewer, 1985], $(\tilde{n}/n)^{tor}$ better fits the experimental results. Near the edge $\tilde{\phi}/(k_b T_e) > \tilde{n}/n$, but in the center the uncertainties are such that they could be equal.

It is important to note that in the presence of counter-propagating fluctuations the HIBP will underestimate the relevant value of $\bar{k}_\theta$. While the usual techniques (except heterodyne FIR scattering) for determining $\bar{k}_\theta$ include contributions from both S_e and S_i, the relevant value of $\bar{k}_\theta$ should consider only S_e. Counter-propagating fluctuations have been seen (the ion feature), but are measured and expected to be at a low level at low $\bar{n}_e$ (the reason for analyzing a low density discharge). Using the measured plasma parameters for the particular discharge predicts no ion feature because $\eta_i = d\ln(T_i)/d\ln(n_i) < 1.5$, the critical value for instability onset. However, the experimental uncertainties allow values of $(\tilde{n}/n)^{\eta_i} \approx 1\%$[Lee, 1986].

b) Particle fluxes

Working particle fluxes in the plasma interior are characterized by both a diffusive term (D^i) and an inward convective term (v^i)[Dnestrovskii, 1985; Gentle, 1987]. An example with large transport coefficients is shown in Fig. 7 for a TEXT discharge, with $v^i \alpha v_0(r/a)^x$, $x \approx 3$, $v_0 \approx 200 ms^{-1}$, and $D^i(\rho<0.4) \approx 2m^2s^{-1}$, $D^i(\rho>0.4) \approx 5m^2s^{-1}$, best fitting the results. In steady state, with no source ($\rho<0.85$), the two terms $-D^i\nabla n$ and nv^i exactly cancel. As was done for the edge plasma, we can measure the electrostatic components of the turbulence, and derive $\Gamma^{f,E}$. The HIBP shows that for $\rho < 0.85$, $\Gamma^i \approx \Gamma^{f,E} \approx 0$ within experimental errors. That is, the electrostatic fluctuations must account for both, or neither, of the two terms $-D^i\nabla n$ and nv^i.

The underlying cause of the interior fluctuations has not been identified, but the broadband feature is often assumed to be due to drift waves. With this assumption we can derive the particle flux Γ^{dw} (or D^{dw} and v^{dw}) using where possible experimental data in theoretical expressions, and compare the predictions with the experimental results (Γ^i, D^i and v^i). The results of the comparison will answer the question "does the measured turbulence, interpreted with the use of a particular theoretical model, explain the measured transport?" The expressions used are given in Table 2. The dissipative trapped electron mode (DTE) is unstable, the universal mode is marginally unstable, and the collisional mode is stable for the measured k_θ values. However, modes deemed stable at the measured k could be excited at higher k and the energy cascade down to the measured k. In

Fig. 7 we show the results of our comparison for the DTE model, incorporating the measured $\tilde{n}/n(k_\theta)$ spectra (with the caveats discussed in the previous section regarding the effects of S_i on the k_θ measurement and scaling). The DTE model predicts an outward convection velocity, with negligible diffusion (because $(k_\theta\rho_s)^2<<1$; however, the turbulent $\Delta\omega$ affects this term). Clearly we still require a (theoretical) inward convection velocity. While the uncertainties in the experimental v^i are large, the neoclassical inward pinch v^{nc}[Howe, 1985], also shown, is too small. Note that the universal mode predicts an inward convection velocity. The ion pressure gradient inward flux[Lee, 1986] is not predicted to be induced in this discharge (because $\eta_i < 1.5$), but the uncertainties in η_i are large.

c) Heat fluxes-electron

To seek correlations between the measured turbulence and q^{tot}_e we must resort to theoretical models. As was done for particle fluxes, we can invoke drift wave models and use the measured values of $\tilde{n}/n(k_\theta)$ in the formulae (Table 2). Such a comparison was first performed by the TFR Group [1983]. An example of the results from TEXT is given in Fig. 8, where the DTE predictions (Table 2) show $q^{dw}_e < q^{tot}_e$. This is in contrast to the results of predictive computer codes[e.g., Romanelli, 1986; Dominguez, 1987] which claim good agreement with experiment in the DTE regime, i.e., they suggest $q^{dw}_e \approx q^{tot}_e$. The difference between the TEXT experimental results and the predictive modeling results is primarily that the measured $\bar{k}_\theta\rho_s \approx 0.1$, rather than ≈ 0.5 as is assumed in the codes. Other tokamaks have found $\bar{k}_\theta\rho_s \approx 0.5$[Liewer, 1985] and this value would lead to approximate agreement between q^{dw}_e and q^{tot}_e in TEXT. This behoves us to better understand the role of the ion feature in the measurements; $S(k,\omega)$, $\bar{k}_\theta$ and $\tilde{n}/n$ include unwanted (for purposes of comparison with drift wave theory) contributions from S_i. However, while accounting for any S_i will increase the relevant $\bar{k}_\theta$, it will decrease the relevant $\tilde{n}/n$ so that the TEXT data will still show $q^{dw}_e < q^{tot}_e$.

Alternative models to explain q_e invoke magnetic fluctuations. If Eq. 9 is applicable, then $\tilde{b}_r/B_\phi$ must decrease from $\approx 10^{-3}$ at the periphery to $\approx 10^{-4}$ near the center. However, existing probe measurements[Ellis, 1985] show $\tilde{b}_r/B_\phi$ increases towards the interior. Nevertheless, appealing correlations between increasing (usually externally measured) $\tilde{b}_r$ and decreasing confinement are often, but not always, found[Robinson, 1986]. An alternative mechanism is proposed by Haas, et al.[see Liewer, 1985], in which the Focker-Planck equation is solved. Here an assumed $\tilde{b}_r/B_\phi$ can be found which is compatible with both the measured $\tilde{n}/n$ and q^{tot}_e.

The observation that χ_e from heat pulse propagation (χ_e^{HP}) exceeds χ_e from power balance (χ_e^{PB}) might be explained by an increased fluctuation driven q_e resulting from gradient changes, in particular ∇T_e. Both FIR scattering and the HIBP have observed enhancements in $\tilde{n}/n$ coincident with sawtooth collapse.

With additional heating, correlations between measured $S(k,\omega)$ and χ_e^{PB} have been found [e.g., TFR Group, 1984]. Although insufficient data exist to make careful comparisons with the predictions of drift wave theories, the results are generally in the correct direction (i.e. $\tilde{n}/n$ increases while χ_e^{PB} increases). A notable exception is PDX[Crowley, 1985] where no change in $S(k,\omega)$ was seen during significant changes in χ_e^{PB} (ohmic to neutral beam heated L mode).

d) Heat fluxes-ion

Unlike the electron heat flux, the ion heat flux is closer to the expected neoclassical value. However, as better ion temperature profiles become available, anomalies (i.e., values inconsistent with neoclassical theory) outside the experimental error bars are being found[Gruebner, 1986]. As the density is increased in ohmic heated discharges a saturation in global energy confinement time τ_E is found[Hugill, 1983]. Figure 9a shows an example from TEXT, where τ_E is linearly dependent on $\bar{n}_e$ for $\bar{n}_e < 5\times10^{19}m^{-3}$. For $\bar{n}_e > 5\times10^{19}m^{-3}$ τ_E saturates. Figure 9b shows the integrated electron and ion energy fluxes as a function of $\bar{n}_e$. Coincident with the saturation of τ_E is an increasing collisional coupling between the electrons and ions, so that the ion channel becomes more important in determining the total energy confinement. If the ions behaved neoclassically the saturation would occur at higher $\bar{n}_e$; the ion losses are anomalous. A mechanism to explain the anomaly is the ion pressure gradient, or η_i, mode, which should appear when η_i exceeds some critical value $\eta_i^{crit} \approx$ 1-2 (we take $\eta_i^{crit} = 1.5$, and $\bar{k}_\theta\rho_s = 0.4$ for S_i). Figure 10 shows a comparison between the experimental and predicted T_i profiles, using either the

neoclassical value χ_i^{nc}[Chang, 1986], $3\chi_i^{nc}$, or $\chi_i^{nc} + \chi_i^{\eta i}$ [Lee, 1986]. For this particular discharge we measure $\eta_i > 1.5$. Using χ_i^{nc} the predicted profile is too broad. Using $3\chi_i^{nc}$ reduces the predicted peak, but the profile remains too broad. Using $\chi_i^{nc} + \chi_i^{\eta i}$ predicts a reduced peak and narrower profile which is more consistent with the experimental results.

If the η_i mode is responsible for the anomalous χ_i, then an ion feature should be observed in the fluctuation spectrum. Figure 11 shows a comparison of the $S(\omega)$ spectra for two discharges, a) at low density, and b) at high density, both with the usual gas puff fueling[Brower, 1987b]. An ion feature (S_i) is seen, whose strength increases as $\bar{n}_e$ increases. This could be a signature of the η_i mode. We do not yet have sufficient information to use measured values of $\tilde{n}/n$ and k (from S_i) in the theoretical expressions for the ion heat fluxes, as we did for drift wave turbulence and electron heat fluxes (e.g., Fig. 8). This comparison is important, because the choice of $\bar{k}_\theta \rho_s$ determines $\chi_i^{\eta i}$.

Peaking the density profile should decrease η_i, reduce $\chi_i^{\eta i}$, and increase τ_E. Such density peaking and concomitant increases in τ_E have been found in most experiments when pellet injection is used.[e.g., Greenwald, 1987].

CONCLUSIONS

In the edge plasma ($\rho > 0.8$) detailed measurements of the various fluctuating quantities density $\tilde{n}$, potential $\tilde{\phi}$, temperature $\tilde{T}$ and magnetic field $\tilde{b}$, together with the various correlations, have been made. The results show broadband turbulence ($\Delta\omega/\bar{\omega}$, $\Delta k_\theta/\bar{k}_\theta > 1$) with frequency $\bar{\omega}/2\pi \approx 100$KHz, poloidal wave number $\bar{k}_\theta \approx 200 m^{-1}$ and parallel wave number $\bar{k}_{||} \approx 1 m^{-1}$. Typical fluctuation levels are $\tilde{n}/n \approx 0.2$, $\tilde{\phi}/(k_b T_e) \approx 0.3$, $\tilde{T}_e/T_e < 0.1$, and $\tilde{b}_r/B_\phi \approx 1 \times 10^{-5}$.

The measurements allow the fluctuation driven particle and heat fluxes to be derived and compared with the total fluxes. The turbulence is responsible for a large part, if not all, of the edge particle fluxes; Γ^i and $\Gamma^{f,E}$ agree in both amplitude and scaling with parameters (B_ϕ, I_p, $\bar{n}_e$, impurity content, E_r). The role of the measured asymmetries should be further investigated. The energy fluxes are apparently less well accounted for by the electrostatic fluctuations, with an unexplained remainder in the conducted heat flux. However, the power balance measurements are not accurate, and it is possible that with $\bar{n}_e > 3 \times 10^{19} m^{-3}$ the electrostatic fluctuations do account for all the energy flux (dominantly convection). At lower densities non-thermal electrons may play a role by increasing the parallel heat flux to the limiter. If there is an unaccounted energy flux, it must be explained by a process which does not significantly affect particle fluxes, because these are already well explained.

The edge turbulence is well characterized, but no completely satisfactory model has been found which predicts all the measured features. The least problematic is the resistivity gradient model, which fails only in its prediction of the m numbers. An up-down asymmetry has been isolated, perhaps a result of toroidal asymmetries, for example, the limiter.

In the plasma confinement region fluctuation measurements are restricted to $\tilde{n}$ and $\tilde{\phi}$ and their correlations. Three distinct features are observed. First is the broadband turbulence, with characteristics similar to those at the edge. Both $\tilde{n}/n$ and $\tilde{\phi}/(k_b T_e)$ decrease towards the plasma center, and $\bar{k}_\theta \rho_s \approx 0.1$ (but with caveats on the interpretation of $\bar{k}_\theta$ because of the possible presence of an ion feature). The fluctuations propagate in the electron diamagnetic drift direction. This feature is often attributed to drift wave turbulence (although v_{ph} is too large) and invoked to explain the experimentally measured heat conduction. Second, a quasi-coherent mode has been identified at the high toroidal field side of the plasma. Again, this feature propagates in the electron diamagnetic drift direction. No theoretical explanation exists, but it is drift-wave like. Third, at high densities, a broadband feature propagating in the ion drift direction is found, which has been associated with the ion pressure gradient driven, or η_i, mode. This mode is used to explain χ_i, which in turn is invoked to explain the saturation of τ_E at high densities.

We have compared the characteristics of the observed fluctuations with the predictions of the models suggested to

explain them. We have also compared the measured plasma transport properties with those predicted to result from the modes, using where possible measured turbulence properties. We find:

1)The broadband fluctuation levels are not generally well represented by mixing length estimates, except near $\rho \approx 0.5$ where $(\tilde{n}/n)^{slab}$ is within a factor ≈ 2 of $(\tilde{n}/n)^{exp}$. Choosing $\bar{k}_\theta \rho_s \approx 0.4$ (instead of the measured ≈ 0.1) brings $(\tilde{n}/n)^{tor}$ within a factor ≈ 2 of $(\tilde{n}/n)^{exp}$.

2)The universal and collisional drift wave modes are respectively marginally unstable and stable at the measured k_θ values.

3)The broadband feature, interpreted as drift wave turbulence (Table 2, DTE), does not explain the usual description of interior particle transport.

4)The broadband feature, interpreted as drift wave turbulence (Table 2, DTE), does not explain the measured interior electron heat flux (unless a k_θ higher than measured is assumed). To continue this (and the particle flux) model and experiment comparison, it is important to understand and correctly interpret the effects of any ion feature. More detailed measurements of $S(k,\omega)$ are required.

5)The measured ion temperatures are approximately predicted using the sum of the neoclassical and pressure gradient driven ion thermal fluxes. The measured ion feature is consistent with the presence of the ion pressure gradient driven mode. The characteristics of the ion feature should be further investigated (e.g., the scalings of $\tilde{n}/n$ and $\bar{k}$) before we can evaluate the relevance of the measured ion feature in determining χ_i.

REFERENCES

Brower, D. L. and others (1985a). *Phys. Rev. Letts.*, 54, 689.
Brower, D. L. and others (1985b). *Phys. Rev. Letts.*, 54, 2579.
Brower, D. L. and others (1987a). *Nucl. Fusion* 27, 2055.
Brower, D. L. and others (1987b). *Phys. Rev. Letts.*, 59, 48.
Chang, C. S. and Hinton, F. L. (1986). *Phys. Fluids* 29, 3314.
Cordey, J. C. and others (1984). *Plasma Physics and Controlled Nuclear Fusion Research* IAEA Vienna, 1, 167.
Crowley, T. and Mazzucato, E. (1985). *Nucl. Fusion* 25, 507.
Dnestrovskii, Yu. N. and others (1984). *Sov. J. Plasma Phys.* 10, 138.
Dominguez, R. R. and Waltz, R. E. (1987). *Nucl. Fusion* 27, 65.
Ellis, J. J. and others (1984). *Plasma Physics and Controlled Nuclear Fusion Research* IAEA Vienna, 1, 363.
Garcia, L. and others (1985). *Phys. Fluids* 28, 2147.
Gentle, K. W. and others (1987). *Plasma Physics and Controlled Fusion* 29, 1077.
Greenwald, M. and others (1986). *Plasma Physics and Controlled Nuclear Fusion Research* IAEA Vienna, 1, 139.
Gruebner, R. J. and others (1986). *Nucl. Fusion* 26, 543.
Howe, H. (1985). ORNL Report, Physics Models in the Tokamak Transport Code PROCTR, ORNL/TM-9537.
Hugill, J. (1983). *Nucl. Fusion* 23, 331.
Lee, G. S. and Diamond, P. H. (1986). *Phys. Fluids* 29, 3291.
Liewer, P. C. (1985). *Nucl. Fusion J.* 25, 543.
Marmar, E. S. and others (1978). *J. Nucl. Mater.* 76 and 77, 59.
Perkins, F. W., *private communication.*
Phillips, P. E. and others (1987). *J. Nucl. Mater.* 145-147, 807.
Powers, E. J. and others (1974). *Nucl. Fusion* 14, 749.
Ritz, Ch. P. and others (1987). *Nucl. Fusion* 27, 1125.
Ritz, Ch. P. and others (1987). FRC report FRCR # 304, Advanced Plasma Fluctuation Analysis Techniques and Their Impact on Fusion Research, University of Texas.
Ritz, Ch. P. and others (1987). *J. Nucl. Mater.* 145-147, 241.
Robinson, D. C. (1986). Turbulence and Anomalous Transport in Magnetized Plasmas, *Cargese Workshop* ed. D. Gresillon and M. Dubois, 21, 1515.
Ross, D. W. and others (1987). FRCR#295, Thermal and Particle Transport in Tokamaks: Theoretical Models for Ignition Studies, University of Texas.
Rowan, W. L. and others (1987). *Nucl. Fusion* 27, 1105.
Similon, P. and Diamond, P. H. (1984). *Phys. Fluids* 27, 916.
Terry, P. W. and others (1985). *Phys. Fluids* 28, 1419.
TFR Group (1983). *Plasma Physics* 25, 641.
TFR Group and Truc, A. (1984). *Plasma Physics and Controlled Fusion* 26, 1045.
Wagner, F. and Lackner, K. (1986). *Physics of Plasma-Wall Interactions in Controlled Fusion* , 931, edited by D. E. Post and R. Behrisch, Plenum Publishing Corporation.
Wesson, J. A. and others (1987). *Plasma Physics and Controlled Nuclear Fusion Research* IAEA Vienna, 2, 3.
Yamada, K. and others (1987). *Nucl. Fusion* 27, 1203.

TABLE 1
A Comparison of Experimental and Theoretical Edge Turbulence Characteristics

	Exp.	collisional ∇n-models	∇_η-models
$\frac{\tilde{n}}{n}$	10 – 50%	$\cong \frac{\rho_s}{L_n}$ or $\frac{1}{k_r L_n} \cong 1 - 20\%$	$\cong T_e^{-5/6} n^{1/3} B_T^{-1/3} q \cong 20\%$
$\frac{e\tilde{\phi}}{k_b T_e}$	$\gtrless \frac{\tilde{n}}{n}$	$\cong \frac{\tilde{n}}{n}$	$\gtrless \frac{\tilde{n}}{n}$
$\frac{\tilde{T}_e}{T_e}$	$\cong (.3 - .5)\frac{\tilde{n}}{n}$	$\frac{\tilde{T}_e}{T_e} \cong 0$	$\cong .3\frac{\tilde{n}}{n}\frac{L_n}{L_{T_e}} \cong (.2 - .4)\frac{\tilde{n}}{n}$ $\cong 5 - 15\%$
$\alpha_{n\phi}$	$.2 - .5\pi$	$\cong 0$	can be large
$\overline{k_\theta}$	$(2 - 3)\text{cm}^{-1}$	$(2 - 3)\text{cm}^{-1}$	$\cong \overline{m}/r \cong 0.5\ \text{cm}^{-1}$
"m-range"	30-100	50-100	≤ 20 for signific. power
$\overline{k_\theta \rho_s}$	$\cong 0.05 - 0.1$	$1 \rightarrow 0.1$	< 0.1
$\overline{k_\parallel}$	$0.005 - .01\text{cm}^{-1}$	$\cong 0$	$\cong \sigma_{k\parallel} \cong \overline{k_\theta}\sigma_r/L_s \cong \{.005\ \text{cm}^{-1}\}$

TABLE 2: Drift Wave Transport Coefficients

$$Q_e = -3/2 P_e \left(\frac{cT_e}{eB}\right) \sum_{ky} \text{Im}\left[\frac{e\phi_k^*}{T_e}\frac{P_e(k)}{P_e}\right] \qquad \text{Total heat flux}$$

$$\Gamma_e = -n_e \left(\frac{cT_e}{eB}\right) \sum_{ky} \text{Im}\left[\frac{e\phi_k^*}{T_e}\frac{n_e(k)}{n_e}\right] \equiv n_e \left(\frac{cT_e}{eB}\right) \sum_{ky} ky \left|\frac{e\phi_k}{T_e}\right|^2 \delta_e(k) \qquad \text{particle flux}$$

$$c_e = Q_e - 5/2 \Gamma_e T_e \equiv n_e T_e \left(\frac{cT_e}{eB}\right) \sum_{ky} ky \left|\frac{e\phi_k}{T_e}\right|^2 \xi_e(k) \qquad \text{conductive heat flux}$$

(5/2 convention)

$$\alpha_k = -\tan^{-1}(\delta_e(k)) \qquad \text{phase angle}$$

Regime	Applicability	$\delta_e(k)$	$\xi_e(k)$
Collisional	$\nu_* = \frac{\nu_e}{\epsilon\omega_{be}} > \frac{\lambda_\parallel}{\lambda_{mfp}} > 1$ $\omega_{be} \equiv \frac{\epsilon^{1/2} v_e}{qR}$, $\epsilon = \frac{r}{R}$, $v_e = \left(\frac{2T_e}{me}\right)^{1/2}$	$\frac{2}{\pi^{1/2}} A^{3/5} \left[\frac{k_\perp^2 \rho_s^2}{1 + k_\perp^2 \rho_s^2} - \frac{3}{2}\eta_e + 0.21\eta_e A^{-1/5}\right]$ $A = (6\nu_e \omega_* / k_\parallel^2 v_e^2) \approx 1$	$\frac{2}{\pi^{1/2}} A^{3/5} \left[\frac{k_\perp^2 \rho_s^2}{1 + k_\perp^2 \rho_s^2}\left(\frac{1}{2} - 0.21 A^{-1/5}\right)\right.$ $\left. -\eta_e(4.06 - 0.83 A^{-1/5})\right]$
Universal	$\frac{\lambda_\parallel}{\lambda_{mfp}} < 1 < \nu_*$	$\pi^{1/2} \frac{\omega_*}{\lvert k_\parallel \rvert v_e} \left[\frac{k_\perp^2 \rho_s^2}{1 + k_\perp^2 \rho_s^2} - 1/2\eta_e\right]$	$\frac{\pi^{1/2}}{2} \frac{\omega_*}{\lvert k_\parallel \rvert v_e} \left[\frac{-3k_\perp^2 \rho_s^2}{1 + k_\perp^2 \rho_s^2} + \frac{7}{2}\eta_e\right]$
Dissipative trapped electron	$\frac{\lambda_\parallel}{\lambda_{mfp}} < \nu_* < 1$; $\nu_{eff} > \omega_*$	$\frac{4}{\pi^{1/2}} \epsilon^{3/2} \frac{\omega_*}{\nu_e} \left[\frac{k_\perp^2 \rho_s^2}{1 + k_\perp^2 \rho_s^2} + \frac{3}{2}\eta_e\right]$	$\frac{4}{\pi^{1/2}} \epsilon^{3/2} \frac{\omega_*}{\nu_e} \left[\frac{1/2 k_\perp^2 \rho_s^2}{1 + k_\perp^2 \rho_s^2} + \frac{15}{4}\eta_e\right]$

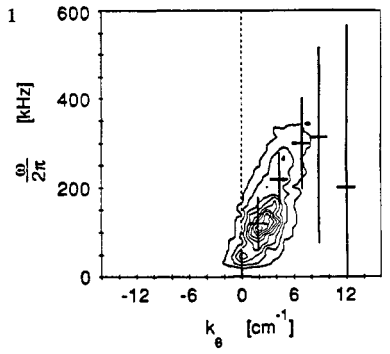

Fig. 1. The $S(k_\theta,\omega)$ spectrum at r = 0.255m in TEXT, from Langmuir probes (contours) and FIR scattering (bars indicate FWHM).

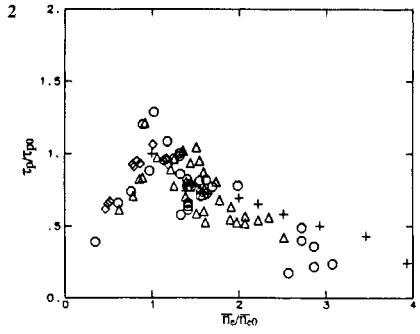

	JET(Δ)	ALC(0)	JT60(+)	TEXT(◊)
τ_{po}(ms)	950	7.8	140	7.3
$\bar{n}_{eo}/10^{19}(m^{-3})$	1.1	14	1.0	3.9

Fig. 2. The density ($\bar{n}_e$) dependence of global particle confinement time (τ_p) for 4 ohmic heated tokamaks. Both τ_p and $\bar{n}_e$ are normalized to the values at which τ_p is a maximum. Relevant parameters for each machine are tabulated.

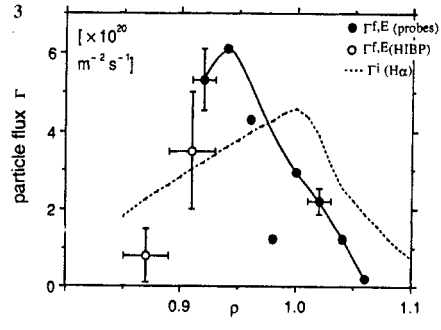

Fig. 3. A comparison of working particle fluxes in TEXT (B_ϕ = 2T, I_p = 200KA, $\bar{n}_e = 3\times10^{19}m^{-3}$, H^+), the total Γ^i (from H_α) and $\Gamma^{f,E}$ driven by electrostatic turbulence. $\Gamma^{f,E}$ is measured with Langmuir probes (solid line, solid points) and the HIBP (open points).

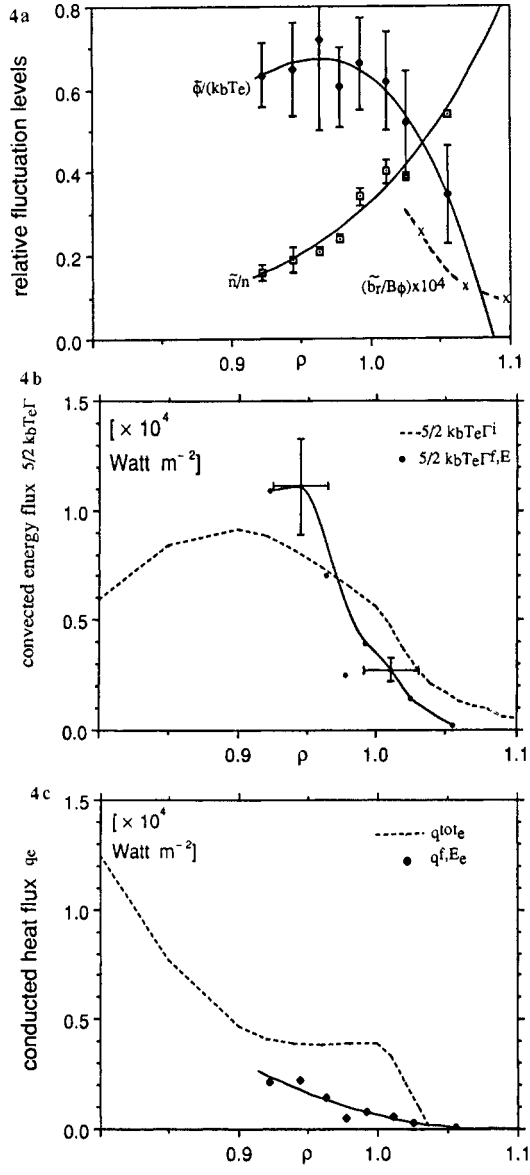

Fig. 4. a) Spatial profiles near the limiter of $\tilde{n}/n$, $\tilde{\phi}/(k_bT_e)$ and $\tilde{b}_r/B_\phi$ measured with probes in TEXT (B_ϕ = 2T, I_p = 200KA, $\bar{n}_e = 3\times10^{19}m^{-3}$, H^+), b) the total ($5/2k_bT_e\Gamma^i$) and electrostatic fluctuation driven ($5/2k_bT_e\Gamma^{f,E}$) convected energy flux, and c) the total (q^{tot}_e) and electrostatic fluctuation driven ($q^{f,E}_e$) conducted electron heat flux.

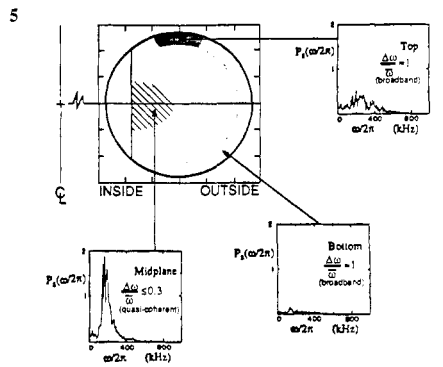

Fig. 5. A cartoon of the turbulence from FIR scattering results on TEXT. The density of points is intended to represent the amplitude of $\tilde{n}/n$. Also shown are the scattered power (P_s) frequency spectra for $k_\perp = 1mm^{-1}$, with the interaction volume along a vertical chord at R=0.95m (50mm inside of the magnetic axis) above, on and below the midplane ($B_\phi = 2.8T$, $I_p = 300KA$, $\bar{n}_e = 4x10^{19}m^{-3}$, H^+).

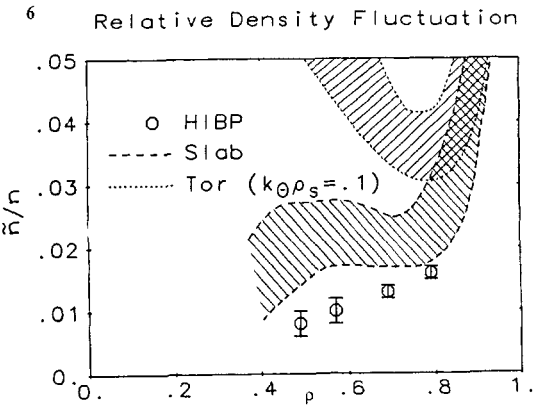

Fig. 6. The spatial profile of $\tilde{n}/n$ from TEXT ($B_\phi = 2T$, $I_p = 200KA$, $\bar{n}_e = 3x10^{19}m^{-3}$, H^+), shown as points (HIBP). Also shown are the predictions of two mixing length estimates, $(\tilde{n}/n)^{tor}$ and $(\tilde{n}/n)^{slab}$. Both $\tilde{n}/n$ and k_θ ($\bar{k}_\theta\rho_s = 0.1$) are interpreted assuming no ion feature.

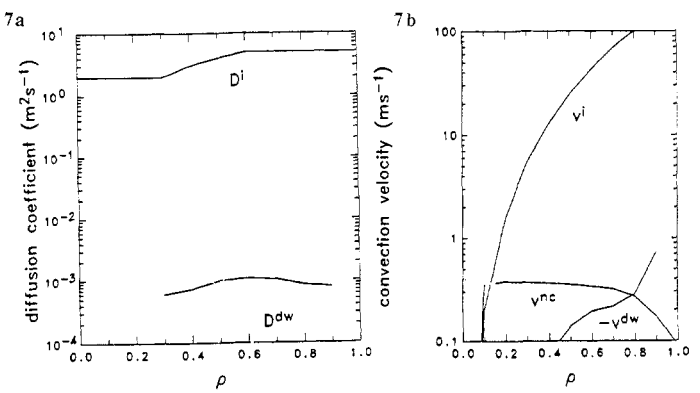

Fig. 7. The spatial variation of a) working particle diffusion coefficient D^i and b) inward convection velocity v^i from oscillating gas puff experiments on TEXT ($B_\phi = 2T$, $I_p = 200KA$, $\bar{n}_e = 2x10^{19}m^{-3}$, H^+). Also shown are the predictions of neoclassical theory (v^{nc}) and drift wave turbulence (DTE) using HIBP measured turbulence properties (D^{dw}, v^{dw}, evaluated using the measured $S(k,\omega)$, with both $\tilde{n}/n$ and $k_\theta\bar{k}_\theta\rho_s = 0.1$) interpreted assuming no ion feature).

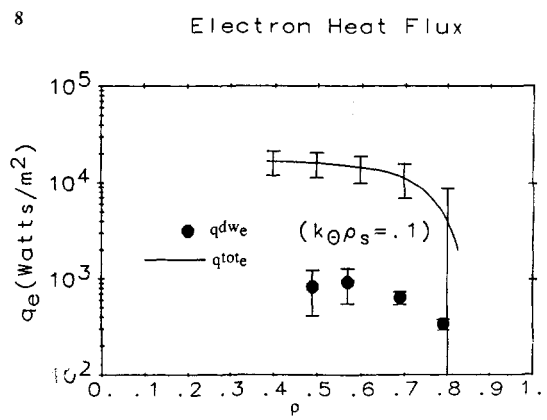

Fig. 8. The radial dependence of the experimental (from power balance) conducted electron heat flux q^{tot}_e in TEXT ($B_\phi = 2T$, $I_p = 200KA$, $\bar{n}_e = 3x10^{19}m^{-3}$, H^+), and the prediction of drift wave turbulence (DTE) q^{dw}_e using experimentally measured characteristics (HIBP measured $S(k,\omega)$, with both $\tilde{n}/n$ and k_θ ($\bar{k}_\theta\rho_s = 0.1$) interpreted assuming no ion feature).

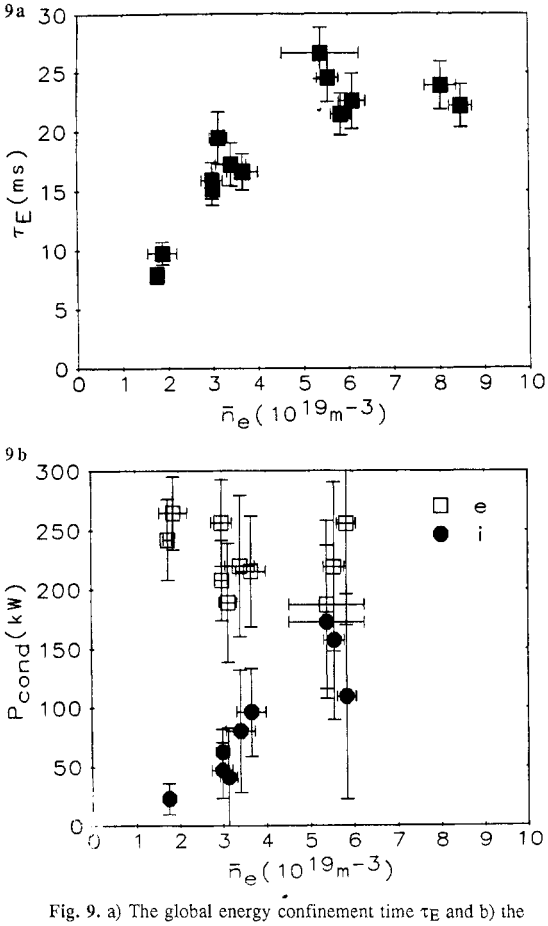

Fig. 9. a) The global energy confinement time τ_E and b) the radially integrated electron and ion conducted powers at ρ =0.6, as functions of density ($\bar{n}_e$ from TEXT (B_ϕ = 2.8T, I_p = 300KA).

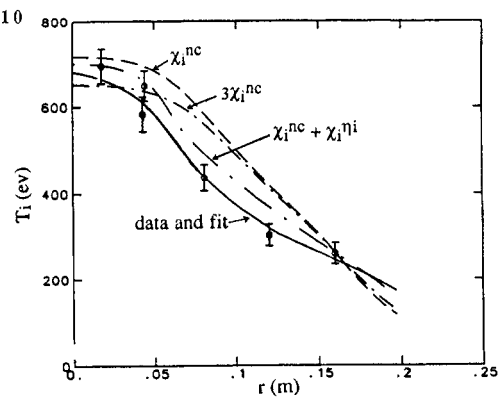

Fig. 10. A comparison between the experimental and predicted T_i profiles, using the neoclassical value χ_i^{nc}, $3\chi_i^{nc}$, and $\chi_i^{nc} + \chi_i^{\eta i}$ (B_ϕ=2.8T, I_p=300KA, ($\bar{n}_e$ =3x10^{19}m^{-3}).

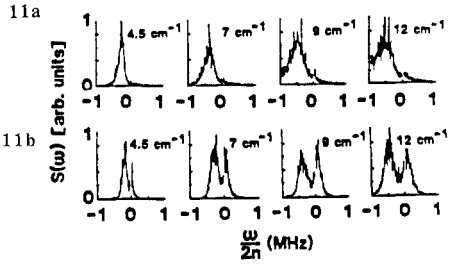

Fig. 11. The power spectrum S(ω) in arbitrary units for four different kθ vectors taken with FIR scattering on TEXT: a) low density gas puff (B_ϕ = 2.8T, I_p = 400KA, $\bar{n}_e$ = 2x10^{19}m^{-3}) and b) high density gas puff (B_ϕ = 2.8T, I_p = 400KA, $\bar{n}_e$ = 8x10^{19}m^{-3}). Negative frequencies correspond to propagation in the electron diamagnetic drift direction.